IEEE Photonics Journal
An IEEE Photonics Society Publication

Open Access

Enhanced Penetration of Human Placental Tissue by SiO_2 Nanoparticles as a Result of Microneedle and Electroporation Treatments

Volume 9, Number 1, February 2017

Panchun Gu
Huajiang Wei
Guoyong Wu
Zhouyi Guo
Hongqin Yang
Yonghong He
Shusen Xie

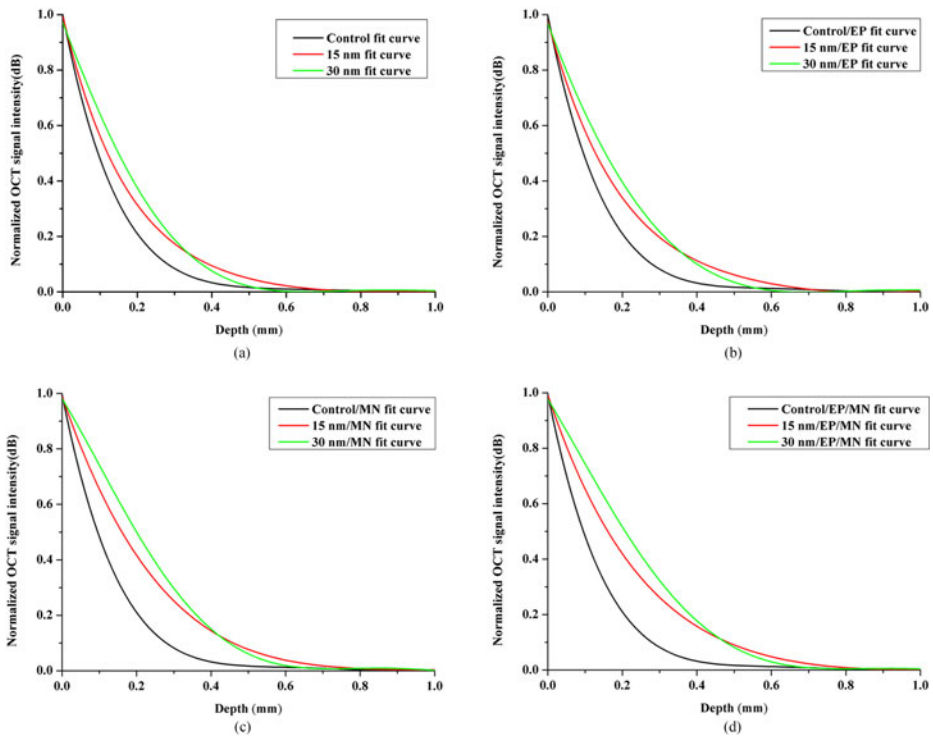

DOI: 10.1109/JPHOT.2017.2649224
1943-0655

Enhanced Penetration of Human Placental Tissue by SiO_2 Nanoparticles as a Result of Microneedle and Electroporation Treatments

Panchun Gu,[1] Huajiang Wei,[1] Guoyong Wu,[2] Zhouyi Guo,[1] Hongqin Yang,[3] Yonghong He,[4] and Shusen Xie[3]

[1]MOE Key Laboratory of Laser Life Science and Institute of Laser Life Science, College of Biophotonics, South China Normal University, Guangzhou 510631, China
[2]Department of Surgery, First Affiliated Hospital, Sun Yat-Sen University, Guangzhou 510080, China
[3]Key Laboratory of Optoelectronic Science and Technology for Medicine of Ministry of Education of China, Fujian Normal University, Fuzhou 350007, China
[4]Graduate School at Shenzhen, Tsinghua University, Shenzhen 518055, China

DOI:10.1109/JPHOT.2017.2649224

Manuscript received November 29, 2016; revised December 21, 2016; accepted January 3, 2017. Date of publication January 10, 2017; date of current version January 19, 2017. This work was supported in part by the National Natural Science Foundation of China under Grant 60778047 and Grant 61275187; in part by the Science and Technology Program of Guangzhou, China, under Grant 201607010371; in part by the Specialized Research Fund for the Doctoral Program of Higher Education of China under Grant 20114407110001; in part by the Natural Science Foundation of Guangdong Province of China under Grant 06025080 and Grant 9251063101000009; in part by the Key Science and Technology Project of Guangdong Province of China under Grant 2005B50101015 and Grant 2008B090500125; in part by the Key Science and Technology Project of Guangzhou City of China under Grant 2008Z1-D391; and in part by the Key Laboratory of Optoelectronic Science and Technology for Medicine (Fujian Normal University), Ministry of Education, China, under Grant JYG1202. Corresponding author: H. Wei (e-mail: weihj@scnu.edu.cn)

Abstract: The objective of this paper is to evaluate the penetration and accumulation of SiO_2 nanoparticles (NPs) in vitro human placental tissue as a function of NP size and electroporation (EP) and microneedle (MN) treatments. The results show that the penetration and accumulation of SiO_2 NPs has a significant influence on the optical properties. Optical coherence tomography (OCT) monitoring and diffuse reflectance (DR) spectra measurements indicate that 30 nm SiO_2 NPs have a tendency to generate greater signal intensities, while 15 nm NPs penetrated faster and had a higher penetration depth. The reduction in average attenuation coefficients of human placental tissue when the SiO_2 NPs size is constant is found to show the following trend: SiO_2 NPs in combination with EP and MN treatment $>$ SiO_2 NPs in combination with MN $>$ SiO_2 NPs with EP $>$ only SiO_2 NPs. It can be concluded that EP and MN treatments dramatically increase the penetration of SiO_2 NPs into human placental tissue. The results prove that OCT and DR spectra can be combined with EP and MN treatments to establish a theoretical basis for the safe use of SiO_2 NPs on human placental tissue and can potentially become a powerful tool for early diagnosis and monitoring of tissue diseases.

Index Terms: $SiO_{\{2\}}$ nanoparticle, human placenta tissue, microneedle, electroporation, optical coherence tomography, diffuse reflectance spectra.

1. Introduction

Nanoparticles (NPs) exhibit unique physical and chemical properties and have received increased attention in recent years because of their potential utility in numerous physical, biological, biomedical, and pharmaceutical applications [1], [2]. Recent observations in biotic systems suggest that particle size can affect the nonspecific uptake of NPs into tissue by influencing the adhesion interactions with tissue [3], [4].

Silica is a widely used nanomaterial in industrial applications such as catalysis, pigments, pharmaceuticals, food additives, electronics, and thin film substrates, because of its facile production and relatively low cost [5]–[7]. Nano-silica can float in air and enter the human body through the respiratory system, skin contact, injection, interventional therapy, or other routes [8], [9]. Once inside the body, silica NPs can enter areas such as liver tissue, lung tissue, and placental tissue through blood circulation [10]–[12]. If pregnant women are exposed to nano-silica during pregnancy, the particles can cross the placental barrier and enter into the fetus. Furthermore, nano-silica can accumulate in the placental tissue and affect fetal development [13], [14]. In addition to playing a fundamental and essential role in fetal development, nutrition, and tolerance, the human placenta may also represent a reserve of progenitor cells. Furthermore, the placenta, which is involved in maintaining fetal tolerance, contains cells that display immunomodulatory properties [15], [16]. Therefore, it is important to study the effect of penetration and accumulation of silica NPs on human placental tissue.

Silica NPs are known to exhibit distinctive optical properties [17]. Therefore, the optical properties of human placental tissue will change as a result of penetration and accumulation of SiO_2 nanoparticles. Several imaging techniques have been applied to study the permeation and accumulation of NPs in biological tissues, including magnetic resonance imaging (MRI), optical projection tomography (OPT), and optical coherence tomography (OCT) [18]–[22]. OCT, a noninvasive technology for micro-structural imaging of biological tissues, has many advantages over other popular imaging systems such as X-ray and magnetic resonance imaging. The benefits include greater safety, lower cost, and enhanced contrast and resolution [23], [24]. Consequently, it has been used to quantify the permeability of a hyper-osmotic agent in atherosclerotic vascular tissue, cancerous gastric tissue, breast cancer tissue, sclera, and skin tissues under both ex-vivo and in-vivo experimental conditions [25]–[28].

Another noninvasive method widely used in monitoring analyte concentrations in tissue and investigating tissue optical parameters is measurement of diffuse reflectance [29], [30]. The technique is rapid, cost effective, requires minimal sample preparation, can be utilized in situ, and is non-destructive. Furthermore, no hazardous chemicals are used, and most importantly, several properties can be measured from a single scan [31]. Taking into account the strengths of the above methods, we decided to use OCT and diffuse reflectance to monitor the process of SiO_2 NPs penetration and accumulation in human placental tissue in this paper.

To further investigate the interactions between SiO_2 NPs and human placental tissue, we also made use of a new physical combination method which uses both a microneedle roller and electroporation to change tissue status. This method can improve the penetration of SiO_2 NPs into human placental tissue. At present, diagnostic and therapeutic technologies that exploit commonly used micro and NPs for medical applications remain a subject of intense research [32]. Most biotherapeutics and vaccines are injected using a hypodermic needle. The microneedle can also be employed for this task, and can be used to introduce NPs into human tissue [33]. Electroporation is a microbiology technique in which an electrical field is applied to cells in order to increase the permeability of the cell membrane, allowing chemicals, drugs, and DNA to be inserted into the cell [34].

In order to assess the interactions between SiO_2 NPs and human placental tissue, in this study we continuously monitored two SiO_2 NPs samples with different particle sizes as they penetrated and accumulated in placental tissue. As mentioned above, monitoring was done with OCT and diffuse reflectance measurements. In addition, microneedle treatment and electroporation were used to enhance the number of SiO_2 NPs penetrating into the tissue, and the effects were studied.

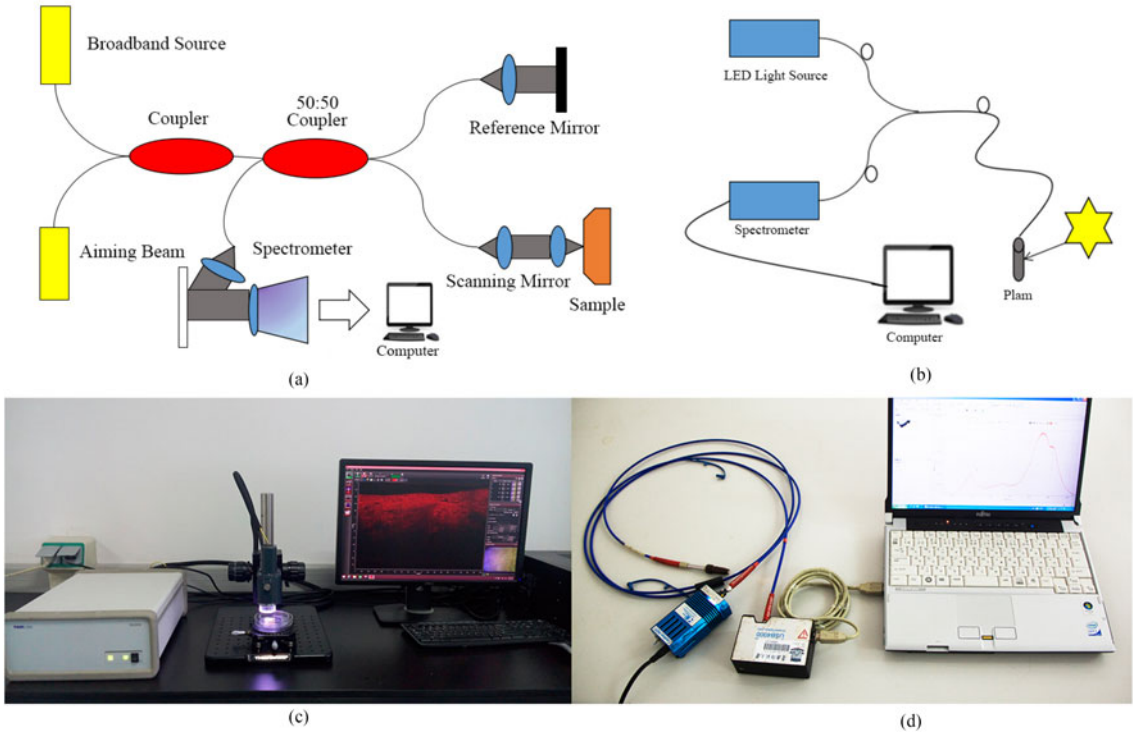

Fig. 1. Schematic diagram of the (a) OCT system and (b) optical fiber spectrometer. (c) OCT system and (d) optical fiber spectrometer.

2. Materials and Methods

2.1 OCT System and Diffuse Reflectance Spectra

In this paper, we used a portable spectral domain OCT system with a central wavelength of 840 nm, bandwidth of 80 nm, in-depth resolution of 7.8 μm, and lateral resolution of 30 μm. Imaging depth range was 1.8 mm, and the line rate was 36 kHz. The operation of the OCT scanner is completely automated and controlled by a portable personal computer. Two-dimensional OCT images were obtained every second during the experiment and stored in the computer for further processing. The OCT system was manufactured by Shenzhen MOPTIM Imaging Technique Co., Ltd., China. Schematic diagram and image of the OCT system are presented in Fig. 1(a) and (c), respectively. Further details can be found in [35].

An optical fiber spectrometer (Ocean Optics, USA, model: USB 4000) was used for the diffuse reflectance measurements. This system consists of a light source and a fiber-optic probe. The spectral range of the diffuse reflectance spectra was from 400 to 1000 nm. The fiber-optic probe consists of seven fibers with an internal diameter of 0.4 mm and a numerical aperture of 0.2 mm. The central fiber is used for collecting the spectra, and the six surrounding fibers are used for illumination. The distance between the centers of the collection fiber and illuminating fibers was 2.25 mm. Each tissue was placed in a quartz cuvette and attached to its inner wall. The probe was placed at a distance of 2.0 mm from the tissue surface. Raw measurement data were stored in the computer for further processing. Schematic diagram and image of the optical fiber spectrometer are shown in Fig. 1(b) and (d), respectively.

2.2 Experimental Preparation

A total of 36 human placental tissue samples were obtained from 36 pregnant women immediately after delivery. The study protocol was approved by the Ethics Committee of the First Affiliated

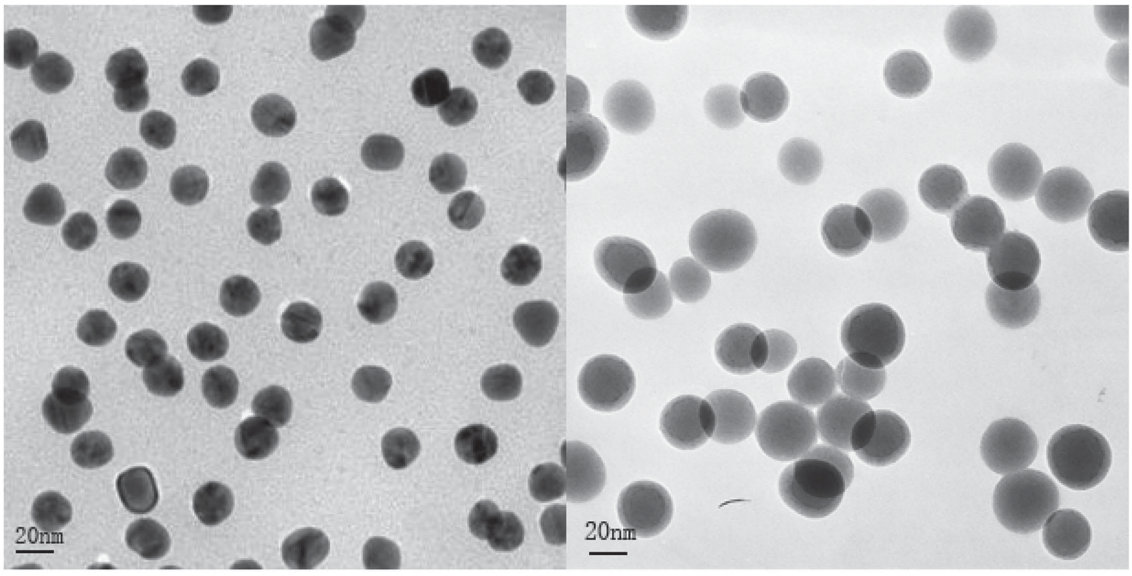

Fig. 2. TEM images of SiO_2 NPs. (a) 15 nm. (b) 30 nm.

Hospital of Sun Yat-Sen University and signed informed consents were obtained from all 36 pregnant women. The tissues were immediately washed with normal saline solution to eliminate excess surface blood after the excision. Then, the tissue samples were stored in a saline container with minimum delay, sealed to prevent spontaneous dehydration, and shipped to the laboratory. Each placental tissue sample was cut into 1.2 cm^2 portions and thawed to room temperature before conducting the investigations.

SiO_2 NPs (Aladdin Chemistry Co, Ltd, Shanghai, China) with average diameters of 15 and 30 nm were used in this work. Transmission electron microscopy (TEM) images of the NPs are given in Fig. 2. A NPs solution was obtained by suspending the SiO_2 NPs powder in distilled water at room temperature at a concentration of 4.0 mg/ml^{-1}. Before the OCT and reflectance spectra measurements, the solution was sonicated for 15-min in order to avoid aggregation.

2.3 Microneedles and Electroporation

In this research, we used a microneedle apparatus with 192 needles. An image of the microneedle apparatus is given in Fig. 3(a). The diameter and length of the microneedles are approximately 0.25 mm and 2.0 mm, respectively. In this work, we applied the microneedle roller for 15 times on the human placental tissue samples.

Electroporation with a frequency of approximately 50–60 MHz and a power of 160 W was applied to the samples immediately after application of the NPs suspension. The pulses were generated by a Dimei medical beauty instrument (Guangzhou, China). The diameter of the probe was approximately 1.1 cm. During electroporation, the probe was immersed in applied physiological saline with sufficient contact pressure. The electroporation instrument is displayed in Fig. 3(b).

2.4 Data Processing

We calculated the attenuation coefficient of human placental tissue from changes in the optical signal intensity during the penetration and accumulation of SiO_2 NPs. The optical attenuation coefficient of the tissue can be quantified from the intensity of the detected light versus the depth. For media with an absorption as described by the single-scattering approximation, the light travels in a ballistic way and Beers law can be applied to calculate the total OCT attenuation coefficient:

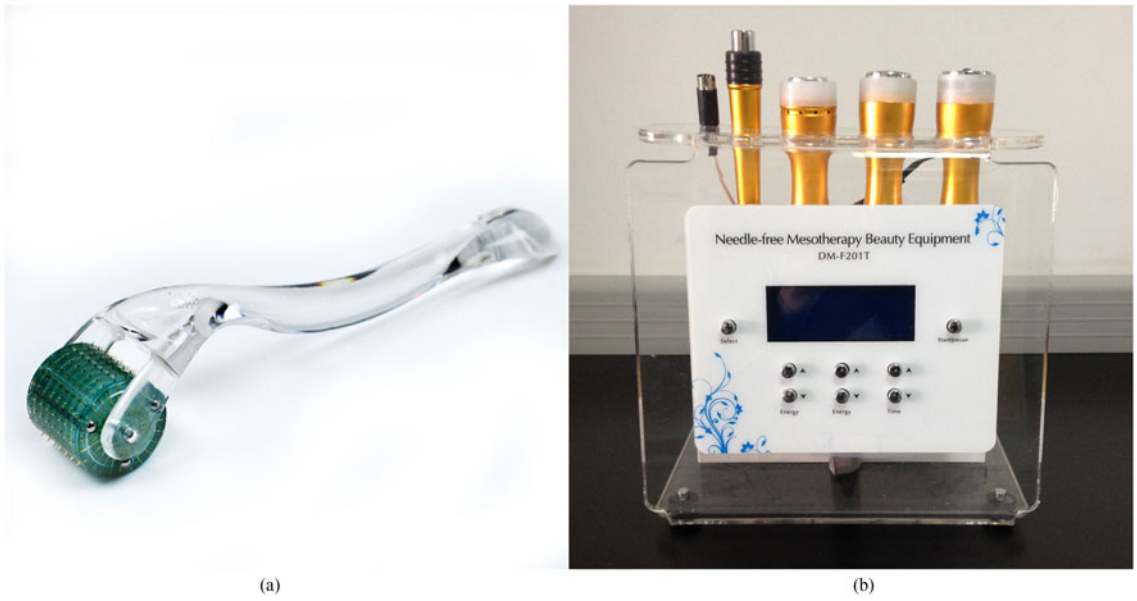

Fig. 3. (a) Microneedle. (b) Electroporation.

$\mu_t = \mu_a + \mu_s$, where μ_a is the absorption coefficient and μ_s is the scattering coefficient. These are physical properties unique to the biological tissue, which play a vital role in the assessment of the tissue feature. In this current OCT system case, the measured signal is defined as [36], [37], [40]:

$$\left[\left\langle i^2(z)\right\rangle\right]^{\frac{1}{2}} \approx \left(\left\langle i^2\right\rangle_0\right)^{\frac{1}{2}} \left[\exp\left(-2\mu_t z\right)\right]^{\frac{1}{2}} \tag{1}$$

where $\left\langle i^2(z)\right\rangle$ the photo detector heterodyne signal is current received by the OCT system from the probing depth z and $\left\langle i^2\right\rangle_0$ is the mean square heterodyne signal. The result of the OCT study is the measurement of optical backscattering or reflectance $R(z) \propto \left[\left\langle i^2(z)\right\rangle\right]^{\frac{1}{2}}$ from a tissue versus axial ranging distance or depth, z. The reflectance depends on the optical properties of the tissue, i.e. the total attenuation coefficient μ_t. Thus, combined with equation (1) and R(z) it follows that the reflected power is approximately proportional to -μ_t z in exponential scale according to the single scattering model

$$R(z) = I_0 a(z) \times (-\mu_t z) \tag{2}$$

where I_0 is the optical power launched into the tissue sample, and a(z) is the reflectivity of the tissue sample at the depth of z. Therefore, measurement of OCT reflectance for depths z_1 and z_2 allows for the approximate evaluation of the attenuation coefficient and its temporal behaviour. This evaluation is due to the reduction of the tissue scattering coefficient at the nanoparticles penetration and accumulation if reflectivity a(z) is considered as weakly dependent on depth for a homogeneous tissue layer. The derivation of the formulas can be found in the literature [36], [37]. The attenuation coefficient μ_t can be theoretically obtained from the reflectance intensity measurements at two different depths z_1 and z_2:

$$\mu_t = 1/\Delta z \times ln[R(z_1)/R(z_2)] \tag{3}$$

where $\Delta z = |z_1 - z_2|$, and R (z) is the reflected power.

Fig. 4 shows an example for calculating the attenuation coefficients of the human placental tissue based on the changes in optical intensity during the penetration and accumulation of SiO_2 NPs. The 'region of interest' in the exponential best fit curve was used to calculate the attenuation coefficient. The region of interest ranges from a depth of 150 μm to a depth of 300 μm, where the OCT signal intensity shows a smooth decrease.

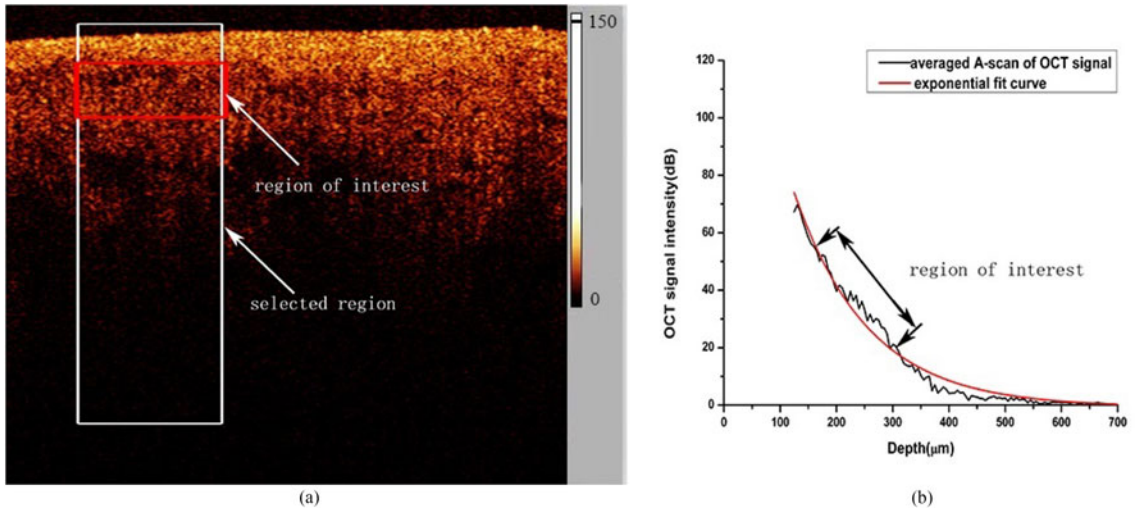

Fig. 4. Typical B-scan of human placental tissue. (a) Range of the selected region and region of interest. (b) Average A-scans (a depth scan of the OCT signal) of the OCT and the exponential best-fit curve.

The data from the human placental tissue samples are given with the standard deviation values calculated by SPSS 10.0 software paired-test. The $p < 0.05$ value indicated high difference.

3. Results and Discussion

The main aim of this research was to monitor the influence of SiO_2 NPs of different sizes penetrating human placental tissue in vitro, under electroporation (EP) and microneedle (MN) treatment, by measuring changes in the tissues' optical properties using OCT imaging and diffuse reflectivity spectral measurements.

Fig. 5 illustrates the exponential best-fit curves for normalized OCT signal intensities, taken 180 min after treatment, of the placental tissues treated with saline, EP, MN, and EP/MN (the measurements were taken after the penetration has reached equilibrium). In the control groups for saline, EP, MN and EP/NM, the OCT signal intensity curves do not change with time. In the samples treated with SiO_2 NPs, the most pronounced changes are increases of the OCT signal intensity and imaging depth over time. This phenomenon is due to the accumulation of SiO_2 NPs in the human placental tissue. This implies that the backscattering intensity of human placental tissue becomes stronger after the application of SiO_2 NPs. The main reason for this is that SiO_2 NPs have strong backscattering and the penetration of SiO_2 NPs increases the backscattering of the human placental tissue with time [38], [39]. As seen in Fig. 5(a), the exponential best-fit curve of the normalized OCT signal intensity of the control is the lowest. The signal intensity of human placental tissue treated for 15 nm with SiO_2 NPs is stronger. The sample treated with 30 nm SiO_2 NPs has an even greater intensity below 330 μm but is lower than the signal from the sample treated with 15 nm SiO_2 NPs at depths over 330 μm. Similarly, among the samples shown in Fig. 5(b),the exponential best-fit curve of normalized OCT signal intensity of the control is the lowest. The next highest signal intensity is from tissue treated with 15 nm SiO_2 NPs in combination with MN, and this is in turn less than for the sample treated with 30 nm SiO_2 NPs combined with MN below 370 μm. However, the signal intensity of samples treated with 15 nm SiO_2 NPs combined with MN is marginally higher than those treated with 30 nm SiO_2 NPs combined with MN at depths over 370 μm. The trends observed in Fig. 5(c) and (d) are the same as in Fig. 5(a) and (b). From Fig. 5, we can come to the conclusion that while 30 nm SiO_2 NPs tend to produce a greater signal intensity, 15 nm NPs penetrate faster and have a higher penetration depth in human placental tissue. The human placental tissue treated with either EP or MN generates much stronger OCT signal intensities than

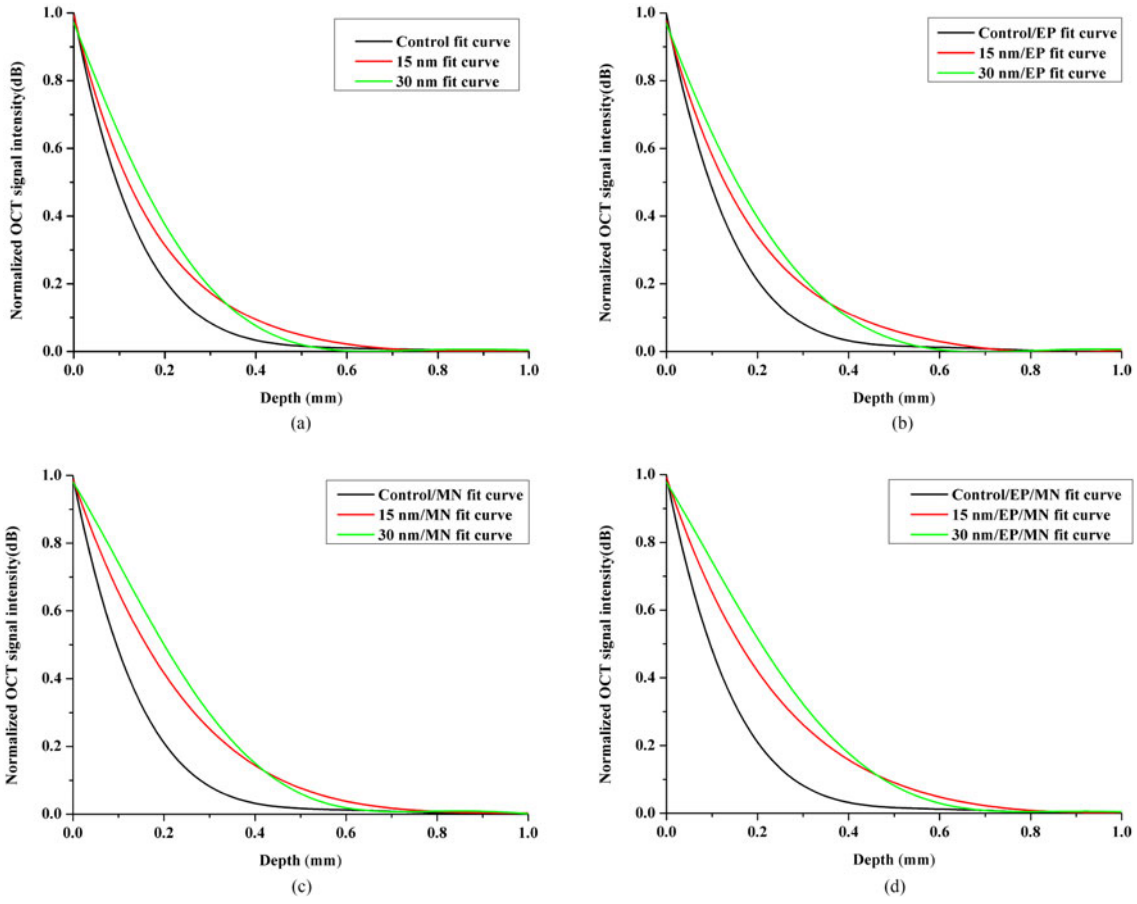

Fig. 5. Exponential best-fit curves of normalized OCT signal intensity taken at 180 min for tissues treated with (a) saline, (b) EP, (c) MN, and (d) EP/MN after the penetration process had reached equilibrium.

untreated tissue. This trend arises due to the effects of EP and MN, which promote penetration of SiO_2 NPs into human placental tissue.

Fig. 6 illustrates the dynamic intensity changes in the diffuse reflectance spectra of the human placental tissue samples after they were topically treated with 15 nm or 30 nm SiO_2 NPs, a combination of 15 nm or 30 nm SiO_2 NPs and EP, a combination of 15 nm or 30 nm SiO_2 NPs and MN, and a combination of 15 nm or 30 nm SiO_2 NPs and EP/MN. The spectra were collected 180 min after treatment, and cover the wavelength range 400–1000 nm. From Fig. 6, it is evident that human placental tissue exhibits prominent absorption bands at wavelengths of approximately 416 nm, 543 nm, and 578 nm [40]. It can be seen from Fig. 6(a) that the average intensity (in the 400–1000 nm range) of the diffuse reflectance spectra of human placental tissue treated with 15 nm SiO_2 NPs in combination with EP/MN is higher than the intensities of tissue samples treated with 15 nm SiO_2 NPs in combination with MN, 15 nm SiO_2 NPs in combination with EP, or 15 nm SiO_2 NPs alone. As seen in Fig. 6(b), samples treated with 30 nm SiO_2 NPs also exhibit similar trends, which arise due to the effects of EP and MN. As mentioned above, these treatments make biological tissue more permeable, and allow more SiO_2 NPs to penetrate into human placental tissue. The penetration effected by a combination of EP and MN is more effective than MN alone, while the latter is more effective than EP. In addition, Fig. 6(a) and (b) suggest that for the samples treated just with NPs, the diffuse reflectance spectral intensity after 180 min is greater in the case of 30 nm SiO_2 NPs when compared to 15 nm SiO_2 NPs. The same trend is observed in the samples treated with SiO_2 NPs in combination with EP, SiO_2 NPs in combination with MN, and SiO_2 NPs in combination

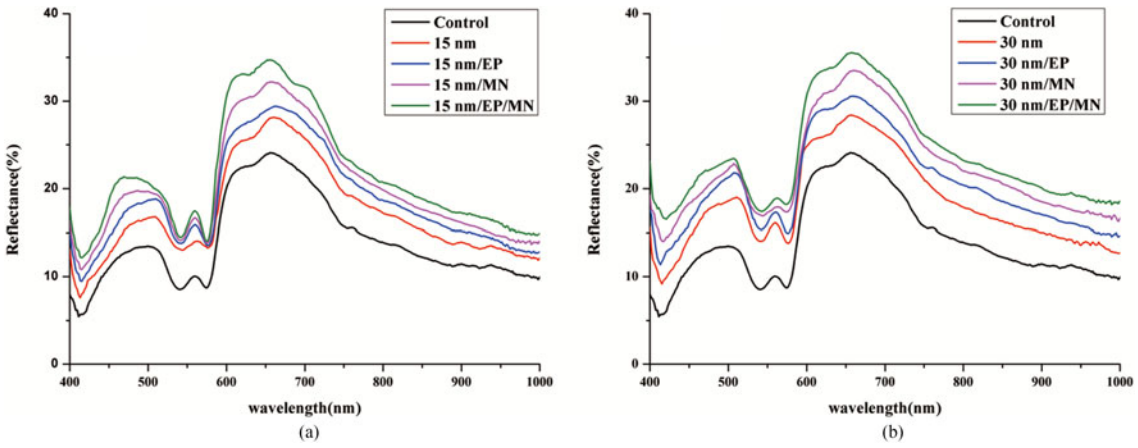

Fig. 6. Diffuse reflectance spectra of the in vitro human placental tissue taken 180 min after the application of (a) 15 nm SiO_2 NPs and (b) 30 nm SiO_2 NPs.

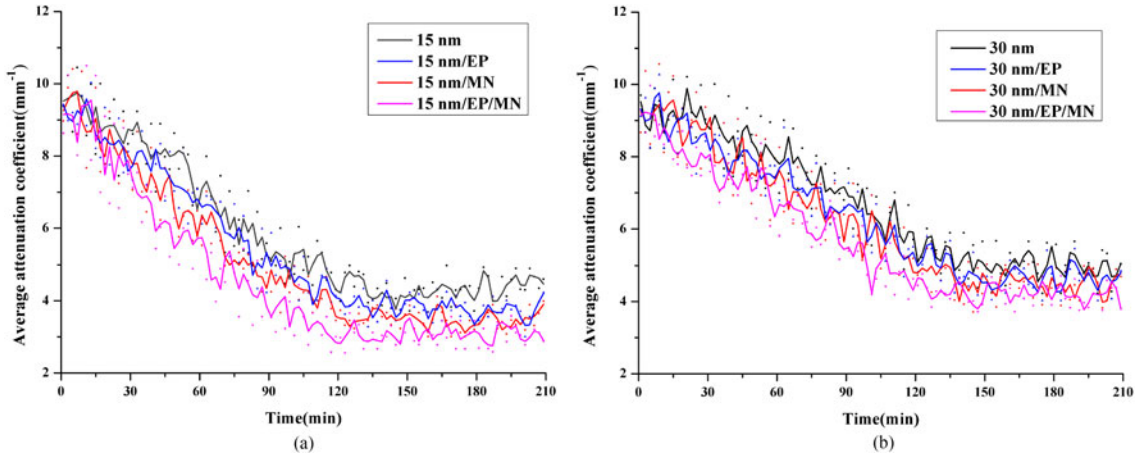

Fig. 7. Average attenuation coefficients of human placental tissue after the application of (a) 15 nm SiO_2 NPs and (b) 30 nm SiO_2 NPs.

with EP/MN. This may be caused by the fact that the 30 nm SiO_2 NPs exhibit larger backscattering than 15 nm SiO_2 NPs, and thus generates a higher intensity in the diffuse reflectance spectra.

To further corroborate the above findings, the attenuation coefficients of the human placental tissue samples were calculated on the basis of the changes to optical intensity. The selected tissue depth region was from 150 to 350 μm, where the OCT signal intensities show comparatively smooth changes.

Fig. 7 summarizes the evolution of the attenuation coefficients of human placental tissue samples that were topically treated with 15 nm or 30 nm SiO_2 NPs, either alone or in combination with EP, MN or EP/MN treatments. As seen in Fig. 7(a), the average attenuation coefficient of human placental tissue is approximately (4.32 ± 0.19) mm^{-1} 142 min after treatment with 15 nm SiO_2 NPs, (3.74 ± 0.17) mm^{-1} 132 min after a combined 15 nm SiO_2 NPs/EP treatment, (3.58 ± 0.16) mm^{-1} 128 min after a combined 15 nm SiO_2 NPs/MN treatment, and (3.16 ± 0.14) mm^{-1} 120 min after a combined 15 nm SiO_2 NPs/EP/MN treatment. The above times represent the point at which the penetration process reached a state of equilibrium. Fig. 7(b) illustrates analogous data for samples treated with 30 nm SiO_2 NPs. The average attenuation coefficients are (5.02 ± 0.24) mm^{-1}, (4.55 ± 0.21) mm^{-1}, (4.42 ± 0.21) mm^{-1}, and (4.19 ± 0.19) mm^{-1} for treatments done with only the NPs, NPs/EP, NPs/MN, and NPs/MN/EP, respectively. The values quoted above are obtained 151 min,

138 min, 133 min, and 123 min after the treatments, respectively, and represent the steady state values.

By comparing the data, it can be concluded that the 15 nm SiO_2 NPs may penetrate faster and reach maximum penetration earlier than the 30 nm SiO_2 NPs under the same conditions. This may be caused by the fact that 30 nm SiO_2 NPs exhibit larger backscattering compared to 15 nm SiO_2 NPs, and thus generate a more substantial increase in the scattering coefficient of the tissue. In addition, for SiO_2 NPs with the same size, the reduction in the attenuation coefficients of the human placental tissue after the various treatments follows the order SiO_2 NPs/EP/MN $>$ SiO_2 NPs/MN $>$ SiO_2 NPs/EP $>$ only SiO_2 NPs. These results indicate that SiO_2 NPs can penetrate more quickly due to the EP and MN treatments.

4. Conclusion

In this paper, we investigated the dynamic changes brought about by penetration and accumulation of SiO_2 NPs with two different sizes in human placental tissue. The changes were observed using OCT imaging and diffuse reflectance spectral measurements. In addition, the influence of EP and MN treatments on SiO_2 NPs penetration was investigated. Our results show that after application of SiO_2 NPs, the OCT signal intensity of human placental tissue increases over time. The larger SiO_2 NPs generate greater OCT signal intensity, while the smaller SiO_2 NPs tend to penetrate deeper and faster into human placental tissue. Moreover, when the NPS size is kept constant, EP and MN enhance NPs penetration and accumulation in human placental tissue. It was also found that the smaller NPs can effect a larger decrease in the attenuation coefficients of the human placental tissue. Overall, we have demonstrated that the OCT technique and DR spectra can be helpful tools for monitoring NPs accumulation in biological tissue. While this study evaluates SiO_2 NPs accumulation in placental tissue, future studies on the impact of SiO_2 NPs on other types of tissue are necessary in order to fully evaluate the potential side effects of this material.

References

[1] K. Shen, Q. Hu, and L. Chen, "Preparation of chitosan bicomponent nanofibers filled with hydroxyapatite nanoparticles via electrospinning," *J. Appl. Polym. Sci.*, vol. 115, no. 5, pp. 2683–2690, 2010.

[2] W. S. Lin, Y. W. Huang, X. D. Zhou, and Y. Ma, "In vitro toxicity of silica nanoparticles in human lung cancer cells," *Toxicol. Appl. Pharmacol.*, vol. 217, no. 3, pp. 252–259, 2006.

[3] F. Lu, S. H. Wu, Y. Hung, and C. Y. Mou, "Size effect on cell uptake in well-suspended, uniform mesoporous silica nanoparticles," *Small*, vol. 5, no. 12, pp. 1–6, 2009.

[4] X. L. Huang, X. Teng, D. Chen, F. Tang, and J. He, "The effect of the shape of mesoporous silica nanoparticles on cellular uptake and cell function," *Biomaterials*, vol. 31, no. 3, pp. 438–448, 2009.

[5] F. F. Zhang *et al.*, "Simultaneous assay of glucose, lactate, L-glutamate and hypoxanthine levels in a rat striatum using enzyme electrodes based on neutral red-doped silica nanoparticles," *Anal. Bioanal. Chem.*, vol. 380, no. 4, pp. 637–642, 2004.

[6] N. Venkatesan, J. Yoshimitsu, Y. Ito, N. Shibata, and K. Takada, "Liquid filled nanoparticles as a drug delivery tool for protein therapeutics," *Biomaterials*, vol. 26, no. 34, pp. 7154–7163, 2005.

[7] M. Qhobosheane, S. Santra, P. Zhang, and W. Tan, "Biochemically functionalized silica nanoparticles," *Analyst*, vol. 126, no. 8, pp. 1274–1278, 2001.

[8] F. Tang, L. Li, and D. Chen, "ChemInform abstract: Mesoporous silica nanoparticles: synthesis, biocompatibility and drug delivery," *Adv. Mater.*, vol. 24, no. 12, pp. 1504–1534, 2012.

[9] S. P. Hudson, R. F. Padera, R. Langer, and D. S. Kohane, "The biocompatibility of mesoporous silicates," *Biomaterials*, vol. 29, no. 30, pp. 4045–4055, 2008.

[10] N. P. V. Til *et al.*, "Kupffer cells and not liver sinusoidal endothelial cells prevent lentiviral transduction of hepatocytes," *Mol. Therapy* vol. 11, no. 1, pp. 26–34, 2005.

[11] M. Harmeet, A. Pallavi, and S. Sanjeev, "Cyclophosphamide disrupts hepatic sinusoidal endothelium and improves transplanted cell engraftment in rat liver," *Hepatology*, vol. 36, no. 1, pp. 112–121, 2002.

[12] Y. Kohei, Y. Yasuo, and H. Kazuma, "Silica and titanium dioxide nanoparticles cause pregnancy complications in mice," *Nature Nanotechnol.*, vol. 6, no. 5, pp. 321–328, 2011.

[13] P. S. Shah and T. Balkhair, "Air pollution and birth outcomes: A systematic review," *Environ. Int.*, vol. 37, no. 2, pp. 498–516, 2011.

[14] D. P. Pope *et al.*, "Risk of low birth weight and stillbirth associated with indoor air pollution from solid fuel use in developing countries," *Epidemiol. Rev.*, vol. 32, no. 1, pp. 70–81, 2010.

[15] M. Paivi and V. Kirsi, "Placental transfer and metabolism: An overview of the experimental models utilizing human placental tissue," *Toxicol. in Vitro*, vol. 27, no. 1, pp. 507–512, 2013.
[16] T. Mose, G. K. Mortensen, M. Hedegaard, and L. E. Knudsen, "Phthalate monoesters in perfusate from a dual placenta perfusion system, the placenta tissue and umbilical cord blood," *ReproductiveToxicol.*, vol. 23, no. 1, pp. 83–91, 2007.
[17] I. A. Rahmana, P. Vejayakumarana, C. S. Sipauta, J. Ismaila, and C. K. Cheeb, "Size-dependent physicochemical and optical properties of silica nanoparticles," *Mater. Chem. Phys.*, vol. 114, no. 1, pp. 328–332, 2009.
[18] K. V. Larin and V. V. Tuchin, "Functional imaging and assessment of the glucose diffusion rate in epithelial tissues in optical coherence tomography," *Quantum Electron.*, vol. 38, no. 6, pp. 551–556, 2008.
[19] M. G. Ghosn, E. Carbajal, N. Befrui, V. Tuchin, and K. Larin, "Differential permeability rate and percent clearing of glucose in different regions in rabbit sclera," *J. Biomed. Opt.*, vol. 13, no. 2, 2008, Art no. 021110.
[20] M. G. Ghosn, N. Sudheendran, M. Wendt, A. Glasser, V. V. Tuchin, and K. V. Larin, "Monitoring of glucose permeability in monkey skin in vivo using optical coherence tomography," *J. Biophoton.*, vol. 3, no. 1/2, pp. 25–33, 2010.
[21] M. G. Ghosn, V. V. Tuchin, and K. V. Larin, "Nondestructive quantification of analyte diffusion in cornea and sclera using optical coherence tomography," *Investigative Ophthalmol. Vis. Sci.*, vol. 48, no. 6, pp. 2726–2733, 2007.
[22] M. G. GHosn, M. Leba, A. Vijayananda, P. Rezaee, J. D. Morrisett, and K. V. Lari, "Effect of temperature on permeation of low-density lipoprotein particles through human carotid artery tissues," *J. Biophoton.*, vol. 2, no. 10, pp. 573–580, 2009.
[23] H. Q. Zhong *et al.*, "Quantification of glycerol diffusion in human normal and cancer breast tissues in vitro with optical coherence tomography," *Laser Phys. Lett.*, vol. 7, no. 4, pp. 315–320, 2010.
[24] R. Sinkus *et al.*, "Imaging anisotropic and viscous properties of breast tissue by magnetic resonance-elastography," *Magn. Reson. Med.*, vol. 53, no. 2, pp. 372–387, 2005.
[25] M. W. Jenkins *et al.*, "Ultrahigh-speed optical coherence tomography imaging and visualization of the embryonic avian heart using a buffered Fourier domain mode locked laser," *Opt. Exp.*, vol. 15, no. 10, pp. 6251–6267, 2007.
[26] K. V. Larin, M. G. Ghosn, S. N. Ivers, A. Tellez, and J. F. Granada, "Quantification of glucose diffusion in arterial tissues by using optical coherence tomography," *Laser Phys. Lett.*, vol. 4, no. 4, pp. 312–317, 2007.
[27] M. G. Ghosn, V. V. Tuchin, and K. V. Larin, "Nondestructive quantification of analyte diffusion in cornea and sclera using optical coherence tomography," *Investigative Ophthalmol. Vis. Sci.*, vol. 48, no. 6, pp. 2726–2733, 2007.
[28] X. Guo *et al.*, "In vivo quantification of propylene glycol, glucose and glycerol diffusion in human skin with optical coherence tomography," *Laser Phys.*, vol. 20, no. 9, pp. 1849–1855, 2010.
[29] R. T. Zaman *et al.*, "In vivo detection of gold nanoshells in tumors using diffuse optical spectroscopy," *Opt. Spectra*, vol. 14, no. 6, pp. 1715–1720, 2007.
[30] D. Fixler and R. Ankri, "Subcutaneous gold nanorods detection with diffusion reflection measurement," *J. Biomed. Opt.*, vol. 18, no. 6, 2013, Art. no. 061226.
[31] R. A. V. Rossel and R. M. Lark, "Improved analysis and modelling of soil diffuse reflectance spectra using wavelets," *Eur. J. Soil Sci.*, vol. 60, no. 3, pp. 453–464, 2009.
[32] E. A. Genina *et al.*, "Fractional laser microablation of skin aimed at enhancing its permeability for nanoparticles," *Quantum Electron.*, vol. 41, no. 5, pp. 396–401, 2011.
[33] E. A. Genina *et al.*, "Transcutaneous delivery of micro- and nanoparticles with laser microporation," *J. Biomed. Opt.*, vol. 18, no. 11, 2013, Art. no. 111406.
[34] E. Neumann, M. Schaeferridder, and Y. Wang, "Gene transfer into mouse lyoma cells by electroporation in high electric fields," *Embo J.*, vol. 1, no. 7, pp. 841–845, 1981.
[35] X. Guo *et al.*, "In vivo comparison of the optical clearing efficacy of optical clearing agents in human skin by quantifying permeability using optical coherence tomography," *Photochem. Photobiol.*, vol. 88, no. 3, pp. 311–316, 2012.
[36] D. Levitz *et al.*, "Determination of optical scattering properties of highly-scattering media in optical coherence tomography images," *Opt. Exp.* , vol. 12, no. 2, pp. 249–259, 2004.
[37] Y. Yang *et al.*, "Optical scattering coefficient estimated by optical coherence tomography correlates with collagen content in ovarian tissue," *J. Biomed. Opt.*, vol. 16, no. 9, 2011, Art. no. 090504.
[38] V. Privezentsev, V. Kulikauskas, A. Bazhenov, and E. Steinman, "ZnO nanoparticle formation in Znion implanted SiO_2/Si structure," *Phys. Status Solidi*, vol. 10, no. 1, pp. 48–51, 2013.
[39] T. J. Maloney, D. E. Aspnes, H. Arwin, and T. W. Sigmon, "Spectroscopic ellipsometric and He backscattering analyses of crystalline Si-SiO_2 mixtures grown by molecular beam epitaxy," *Appl. Phys. Lett.*, vol. 44, no. 5, pp. 517–519, 1984.
[40] Y. Q. Zhang *et al.*, "Effect of differently sized nanoparticles accumulation on the optical properties of ex vivo normal and adenomatous human colon tissue with OCT imaging and diffuse reflectance spectra," *Laser Phys. Lett.*, vol. 11, 2014, Art. no. 085901.